Position space formulation for Dirac fermion on honeycomb lattice (蜂の巣格子上でのディラックフェルミオンの実空間定式化)

Masaki Hirotsu

February 27th, 2015

Abstract

Focusing on the analogy between the electron system in graphene and the staggered fermion in lattice gauge theory, we consider an alternative formulation in position space for Dirac fermion on the honeycomb lattice, which can be regarded as a counterpart of the conventional momentum space formulation. In this formulation, we find a hidden exact symmetry on the lattice, which protects the masslessness of Dirac fermion, and show that the symmetry remains exact even if we consider interlayer hopping interaction in bilayer graphene. In lattice gauge theory, our formulation can also be regarded as one of the lattice fermion formalisms, and will present a new direction for studying a construction of lattice fermion.

Contents

1 Introduction

In particle physics, lattice gauge theory has been regarded as a unique method to strictly define quantum field theory without perturbation theory, and significantly contributed to study quantum field theory non-perturbatively. However, as is well known, there is the so-called fermion doubling problem in defining massless Dirac fermion on the lattice, and it is needed to present a formalism which does not conflict the doubling problem, and enables a faster numerical simulation for studying non-perturbative dynamics in quantum field theory. To achieve this, there are a lot of studies of constructing lattice fermions. In condensed matter physics, the emergence of massless Dirac fermion has been observed in some materials recently. The emergence mechanism of Dirac fermion may provide a new hint for constructing lattice fermions. Especially, here we focus on the graphene electron system and introduce an alternative formulation for Dirac fermion on honeycomb lattice in position space based on Ref.[1].

Graphene is a genuine two-dimensional crystal of carbon atoms with a hexagonal lattice [2, 3, 4, 5, 6]. In a theoretical point of view, such low dimensional crystal has been expected to be unstable to thermal fluctuations, and commonly regarded as merely an ideal object for a long time. However, contrary to this expectation, in 2004, K. S. Novoselov, A. K. Geim, et al. have succeeded in isolating a monatomic layer of graphene from highly oriented pyrolytic graphite (HOPG) [2]. This discovery became a breakthrough of recent great progress in graphene physics (also in low dimensional condensed matter physics), and now, graphene attracts much interest in condensed matter physics as well as high energy physics for its remarkable features [8, 9, 10].

One of the most important features of graphene is that the quasiparticle behaves like massless Dirac fermion in the relativistic quantum field theory [3, 4, 5, 6]. The observations of linear dispersion relation [3, 4], and anomalous quantum hall effect [5] imply that the quasiparticle of graphene obeys massless Dirac equation, and this is also consistent with other experimental result [6]. Why does massless Dirac fermion emerge in such non-relativistic many body system? The specific features of graphene had already been studied theoretically before its discovery [11, 12, 13, 14, 15], while the conventional explanation to the above question is presented in Refs.[14, 15]. Particularly, in Ref.[15], starting from the tight-binding model on honeycomb lattice, it is shown that the four component spinor field composed of the low energy excitations around two different Dirac points is regarded as massless Dirac fermion field.

The conventional model gives a clear understanding of the specific electronic structure of graphene. However, this is not the first case in which massless Dirac fermion field is constructed on the lattice. In lattice gauge theory, several types of lattice fermion formalisms to define Dirac fermion formulation on the lattice are known. In particular, the graphene model seems closely analogous to the staggered fermion formalism [18], in which the $2^{[d/2]}$ flavor Dirac fermions are constructed from the Hamiltonian describing the nearest neighbor hopping of single spinless fermion on the $(d-1)$-dimensional hypercubic space lattice. In the staggered fermion formalism, the construction of Dirac fermion formulation has been studied in momentum space [19, 20, 21] as well as position space [22]. In the momentum space formulation, Brillouin Zone (BZ) is cut into 2^d regions, and each region is reinterpreted as spin-flavor

degrees of freedom of $2^{[(d+1)/2]}$ flavor Dirac fermions. In the position space formulation, the single fermion field is redefined on the fundamental lattice composed of centers of d-dimensional hypercubic unit cells, and the 2^d sites in each unit cell are reinterpreted as spin-flavor degrees of freedom of $2^{[(d+1)/2]}$ flavor Dirac fermions.

In the conventional graphene model in momentum space, Dirac fermion field is defined as four component spinor field composed of the low energy excitations around two different Dirac points which are spatially separated in BZ [15]. Comparing this formulation to the staggered fermion formalism, we notice that the conventional graphene model is analogous to the momentum space formulation in the staggered fermion formalism. Thus, we expect that it may be possible to construct Dirac fermion formulation in position space for graphene.

In this thesis, focusing on the analogy between the electron system in graphene and the staggered fermion in lattice gauge theory, we consider an alternative formulation in position space for Dirac fermion on the honeycomb lattice, which can be regarded as a counterpart of the conventional momentum space formulation [1]. Furthermore, we also present an explicit formulation of exact symmetry, which protects the masslessness of Dirac fermion [1]. This formulation may be useful for studying a non-perturbative dynamics in condensed matter physics such as spontaneous chiral symmetry breaking in suspended graphene [7, 25, 26, 27, 28, 29]. In a point of view of lattice gauge theory, our formulation can also be regarded as one of the lattice fermion formalisms on two-dimensional space lattice. This will be a fist step for extending the graphene model to a four-dimensional hyperdianmond lattice fermion formalism, and may be widely useful for studying other lattice regularization methods on non-hypercubic lattices.

This thesis is organized as follows. In section 2, we introduce a basic review of graphene, and explain the conventional derivation of Dirac fermion formulation on honeycomb lattice in momentum space [15]. In section 3, we present our formulation in position space, and discuss Dirac point and physical modes at the next-leading order of tight-binding approximation. In section 4, we show that massless Dirac fermion appears in the continuum limit after integrating out an unphysical mode. In section 5, we also show that there is a hidden exact symmetry on the lattice, which protects the masslessness of Dirac fermion. In section 6, we extend our formulation to the AB-stacked bilayer graphene system, and show that the symmetry remains exact even if interlayer hopping interaction exists. In the last section, we present the summary and discussion.

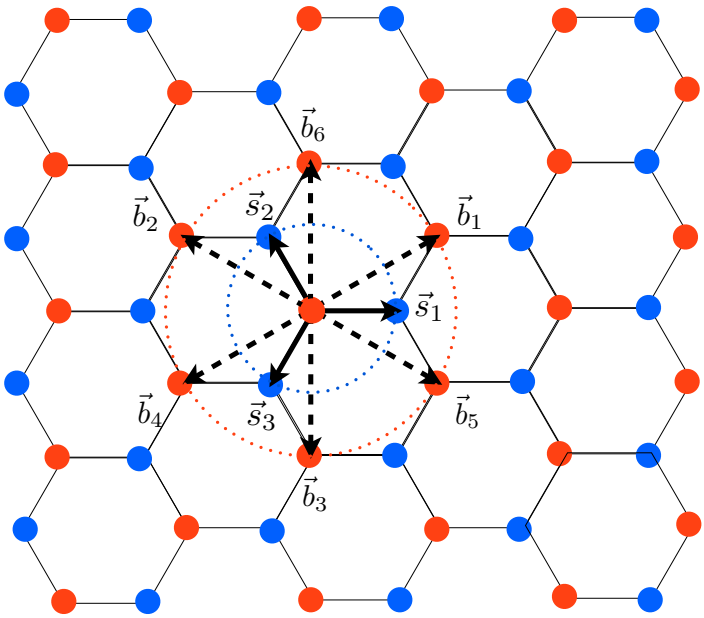

Figure 1: Honeycomb lattice

2 Review of graphene

2.1 Lattice structure

In this section, we introduce a basic review of conventional formulation for Dirac fermion on honeycomb lattice in momentum space [15]. Before that, here we briefly review the lattice structure of graphene.

Graphene is a genuine two-dimensional crystal of carbon atoms with a hexagonal lattice, and it attracts much interest for its remarkable features. In the graphene electron system, four valence electrons of each carbon atom are used for three σ orbitals and one π orbital, and electron career (π electron) hops on the lattice formed by those σ electrons covalent bonding. The lattice structure is seen in carbon allotrope (graphite, carbon nanotube, fullerene), and other two-dimensional condensed matter systems such as silicene, and characterizes the specific electronic structures of those materials as well as graphene.

The honeycomb lattice is constituted of two triangular sublattices A and B (Figure 1). The lattice structure is invariant under $2\pi/3$ rotation in the plane (C_3 symmetry), and also under space inversion in which two sublattice sites A and B can be interchanged (inversion symmetry). The vectors $\vec{s}_i (i = 1, 2, 3)$ in Figure 1 denote the position vectors for three nearest neighbor sites and given as follows;

$$\vec{s}_1 = a_0 \begin{pmatrix} 1, & 0 \end{pmatrix}, \ \vec{s}_2 = a_0 \begin{pmatrix} -1/2, & \sqrt{3}/2 \end{pmatrix}, \vec{s}_3 = a_0 \begin{pmatrix} -1/2, & -\sqrt{3}/2 \end{pmatrix}, \quad (1)$$

where a_0 is the lattice spacing between the nearest neighbor sites, and, in the graphene system, $a_0 \simeq 1.42$ $\mathring{A}$ [10]. The vectors $\vec{b}_j$ $(j = 1, \cdots, 6)$ in Figure 1 denote the

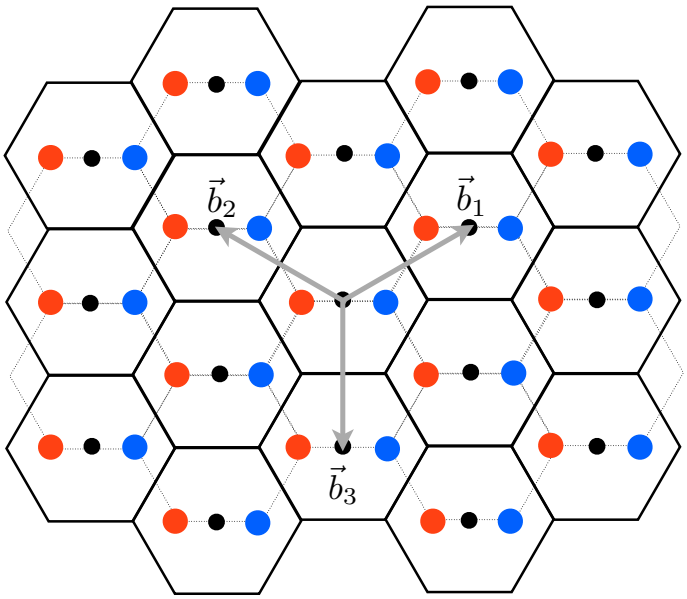

Figure 2: Fundamental lattice

fundamental vectors of honeycomb lattice, and given as follows [a];

$$\vec{b}_1 = a_0 \left(\ 3/2, \quad \sqrt{3}/2 \ \right), \ \vec{b}_2 = a_0 \left(\ -3/2, \quad \sqrt{3}/2 \ \right), \vec{b}_3 = a_0 \left(\ 0, \quad -\sqrt{3} \ \right), \quad (4)$$

$$\vec{b}_4 = a_0 \left(\ -3/2, \quad -\sqrt{3}/2 \ \right), \vec{b}_5 = a_0 \left(\ 3/2, \quad -\sqrt{3}/2 \ \right), \ \vec{b}_6 = a_0 \left(\ 0, \quad \sqrt{3} \ \right). \quad (5)$$

From the Figure 1, one can see that the sublattices A and B are shifted by $\vec{s}_1$ (or $\vec{s}_2$, $\vec{s}_3$), and it is unable to overlap them each other by any translations which are generated by the fundamental vectors $\vec{b}_j$ $(j = 1, \cdots, 6)$. Therefore, there are two independent sites A and B in each unit cell of fundamental lattice (Figure 2). The sublattice degrees of freedom A and B in the unit cell will be reinterpreted as spin degrees of freedom (pseudospin), and plays an important role for understanding the specific features of electron system on the honeycomb lattice.

The reciprocal vectors $\vec{d}_1$, $\vec{d}_2$ are given as follows;

$$\vec{d}_1 = 2\pi/a_0 \left(\ 1/3, \quad 1/\sqrt{3} \ \right), \ \vec{d}_2 = 2\pi/a_0 \left(\ -1/3, \quad 1/\sqrt{3} \ \right), \quad (6)$$

where vectors $\vec{b}_i$ and $\vec{d}_j$ satisfy the following orthogonal relation,

$$\vec{b}_i \cdot \vec{d}_j = 2\pi\delta_{ij} \ (i, j = 1, 2). \quad (7)$$

[a] We note that, using $\vec{s}_i (i = 1, 2, 3)$, the fundamental lattice vectors $\vec{b}_j$ $(j = 1, \cdots, 6)$ is rewritten as follows

$$\vec{b}_1 = \vec{s}_1 - \vec{s}_3, \ \vec{b}_2 = \vec{s}_2 - \vec{s}_1, \ \vec{b}_3 = \vec{s}_3 - \vec{s}_2, \quad (2)$$

$$\vec{b}_4 = \vec{s}_3 - \vec{s}_1, \ \vec{b}_5 = \vec{s}_1 - \vec{s}_2, \ \vec{b}_6 = \vec{s}_2 - \vec{s}_3. \quad (3)$$

There are six edge points in BZ, which are related to K, K' under the C_3 symmetry. The position vectors for K, K' are given as follows;

$$\vec{K} = 2\pi/3a_0 \begin{pmatrix} 1, & 1/\sqrt{3} \end{pmatrix} , \vec{K}' = 2\pi/3a_0 \begin{pmatrix} 1, & -1/\sqrt{3} \end{pmatrix}. \tag{8}$$

In the graphene system, there is one π electron per site on average, and a half of energy eigenstates is occupied (half-filled electron system). In the next section, we show that starting from the tight-binding model on the honeycomb lattice, π electron behaves like massless Dirac fermion in low energy regime [15].

2.2 Conventional derivation of Dirac fermion formulation

2.2.1 Tight-binding model

In this section, we review the conventional formulation for Dirac fermion on honeycomb lattice in momentum space [15]. First, we start from the tight-binding model on the honeycomb lattice. Defining creation (annihilation) operators of quasiparticles on A and B sublattices as $a^\dagger_\sigma(\vec{r})$ ($a_\sigma(\vec{r})$), $b^\dagger_\sigma(\vec{r})$ ($b_\sigma(\vec{r})$), the tight-binding Hamiltonian at the next-leading order is given as follows;

$$\begin{aligned} \mathcal{H} = & - t \sum_{\vec{r}} \sum_{\sigma=\pm} \Big[a^\dagger_\sigma(\vec{r}) b_\sigma(\vec{r}) + b^\dagger_\sigma(\vec{r}) a_\sigma(\vec{r}) + a^\dagger_\sigma(\vec{r}+\vec{b}_1) b_\sigma(\vec{r}) \\ & + b^\dagger_\sigma(\vec{r}-\vec{b}_1) a_\sigma(\vec{r}) + a^\dagger_\sigma(\vec{r}-\vec{b}_2) b_\sigma(\vec{r}) + b^\dagger_\sigma(\vec{r}+\vec{b}_2) a_\sigma(\vec{r}) \Big] \\ & - t' \sum_{\vec{r}} \sum_{j=1}^{6} \sum_{\sigma=\pm} \Big[a^\dagger_\sigma(\vec{r}+\vec{b}_j) a_\sigma(\vec{r}) + b^\dagger_\sigma(\vec{r}) b_\sigma(\vec{r}+\vec{b}_j) \Big], \end{aligned} \tag{9}$$

where the first and second lines correspond to the nearest neighbor hopping term, and the third line corresponds to the next-nearest neighbor hopping term. The argument of fermionic operators $\vec{r}$ denotes a center coordinate of unit cell, and σ denotes a spin index ($\sigma = \pm$). Here, the hopping amplitudes t, t' are given as $t \simeq 2.8$ eV, and $t' \simeq 0.1$ eV in the graphene system [32]. In the following, we neglect the next-nearest neighbor hopping term, and also omit the spin index σ for convenience.

2.2.2 Dispersion relation

Next, in order to show Dirac points, and derive a low energy effective theory, we take the following Fourier representations of $a(\vec{r})$, $b(\vec{r})$;

$$a(\vec{r}) = \int_{BZ} \frac{d^2k}{(2\pi)^2} \tilde{a}(\vec{k}) e^{i\vec{k}\cdot\vec{r}}, \; b(\vec{r}) = \int_{BZ} \frac{d^2k}{(2\pi)^2} \tilde{b}(\vec{k}) e^{i\vec{k}\cdot\vec{r}}. \tag{10}$$

In momentum space, the Hamiltonian at the leading order of tight-binding approximation is represented as follows;

$$\mathcal{H} = -t \int_{BZ} \frac{d^2k}{(2\pi)^2} \begin{pmatrix} \tilde{a}(\vec{k}) \\ \tilde{b}(\vec{k}) \end{pmatrix}^\dagger \begin{pmatrix} 0 & D(\vec{k}) \\ D^*(\vec{k}) & 0 \end{pmatrix} \begin{pmatrix} \tilde{a}(\vec{k}) \\ \tilde{b}(\vec{k}) \end{pmatrix} \tag{11}$$

with

$$D(\vec{k}) = 1 + e^{-i\vec{k}\cdot\vec{b}_1} + e^{i\vec{k}\cdot\vec{b}_2}. \tag{12}$$

Here, the energy spectrum of Hamiltonian (11) is given as follows;

$$E(\vec{k}) = \pm t|D(\vec{k})|. \tag{13}$$

In the half-filled electron system, the all negative energy eigenstates are occupied (Dirac's sea), and the negative and positive energy eigenvalues in Eq.(13) correspond to the valence and conduction band respectively. Thus, Dirac point should appear at zero energy level. The condition, which a wave vector on the Fermi surface fulfills, is given by

$$D(\vec{k}) = 1 + e^{-i\vec{k}\cdot\vec{b}_1} + e^{i\vec{k}\cdot\vec{b}_2} = 0. \tag{14}$$

The above equation is fulfilled when $e^{-i\vec{k}\cdot\vec{b}_1}$,$e^{i\vec{k}\cdot\vec{b}_2}$ equal to ω, ω^* or ω^*, ω, and there appear two independent Dirac points K and K' at the edge of BZ.

Expanding $E(\vec{k})$ around each Dirac point with respect to the momentum, and denoting p as the momentum from each Dirac point, we see

$$E \simeq \pm v_F|\vec{p}|, \tag{15}$$

where $v_F = 3/2a_0t$ is the Fermi velocity. Since the above equation is analogous to the dispersion relation of massless Dirac fermion, these points K, K' are often called as Dirac points, and also the conical dispersion relations are called as Dirac cones. At the Dirac points, the valence band is in touch with conduction band, so that the electron system is gapless.

This specific band structure around Dirac points was originally predicted in Ref.[11] before the discovery of graphene. The appearance of Dirac points is deeply related to some symmetries, and it is known that, under the inversion and C_3 symmetry, Dirac points should appear at K, and K' in BZ [12, 13], and, the inversion and time reversal symmetries protect the stability of Dirac points to small deviations [31].

In some literature in condensed matter physics, an appearance mechanism of Dirac point in other material has been discussed. For instance, in Ref.[17], the relation between Dirac points and symmetries mentioned above is extended to more general cases, and an appearance mechanism of Dirac point in two-dimensional lattices is generally discussed.

2.2.3 Derivation of Dirac fermion formulation

The low energy effective Hamiltonian is derived by expanding $D(\vec{k})$ in Eq.(11) around the Dirac points with respect to the momentum. In the low energy regime, there appear two low energy excitations around the Dirac points. Here, if we introduce the four component spinor field $\tilde{\xi}(\vec{p})$, which is composed of the two low energy excitations, as

$$\tilde{\xi}(\vec{p}) = \left(\tilde{a}(\vec{K}+\vec{p}),\ \ \tilde{b}(\vec{K}+\vec{p}),\ \ \tilde{b}(\vec{K'}+\vec{p}),\ \ \tilde{a}(\vec{K'}+\vec{p}) \right)^T, \tag{16}$$

in the continuum limit, the low energy effective Hamiltonian is derived as follows;

$$\mathcal{H}_0 = v_F \int \frac{d^2p}{(2\pi)^2} \tilde{\xi}(\vec{p})^\dagger \hat{\gamma}_0 [\hat{\gamma}_1 p_x + \hat{\gamma}_2 p_y] \tilde{\xi}(\vec{p}) \tag{17}$$

where p_x, p_y are components of momentum in Cartesian coordinate, and the matrices $\hat{\gamma}_\mu$ $(\mu = 0, 1, 2)$ are defined as

$$\hat{\gamma}_0 = \begin{pmatrix} \sigma_3 & 0 \\ 0 & -\sigma_3 \end{pmatrix}, \ \hat{\gamma}_1 = \begin{pmatrix} -i\sigma_1 & 0 \\ 0 & i\sigma_1 \end{pmatrix}, \ \hat{\gamma}_2 = \begin{pmatrix} -i\sigma_2 & 0 \\ 0 & i\sigma_2 \end{pmatrix}. \tag{18}$$

We note that the coefficients matrices $\hat{\gamma}_\mu$ $(\mu = 0, 1, 2)$ in Eq.(17) satisfy Clifford algebra $\{\hat{\gamma}_\mu, \hat{\gamma}_\nu\} = 2g_{\mu\nu} \cdot 1_{4\times4}$, where $g_{\mu\nu}$ is the metric in (2+1)−dimensional space-time. Thus, starting from the tight-binding model on the honeycomb lattice, we show that the low energy effective Hamiltonian is consistent with the massless Dirac Hamiltonian in (2+1)−dimensional space-time, except for the Fermi velocity v_F. Here, if we introduce an additional matrix $\hat{\gamma}_3$ anti-commuting with $\hat{\gamma}_0$, $\hat{\gamma}_1$, $\hat{\gamma}_2$, where we have the following two choices for $\hat{\gamma}_3$ as

$$\begin{pmatrix} 0 & 1_{2\times2} \\ -1_{2\times2} & 0 \end{pmatrix}, \begin{pmatrix} 0 & -i\ 1_{2\times2} \\ -i\ 1_{2\times2} & 0 \end{pmatrix}, \tag{19}$$

and define

$$\hat{\gamma}_5 = i\hat{\gamma}_0\hat{\gamma}_1\hat{\gamma}_2\hat{\gamma}_3, \tag{20}$$

we also derive the flavor-chiral symmetry, which protects the masslessness of Dirac fermion [1, 16]. In Eq.(17), the four components spinor is decomposed into two Weyl spinors, so that the Dirac fermion is also regarded as two Weyl fermions with opposite chiralities. This is known as the so-called fermion doubling in lattice gauge theory, and, in the graphene system, those fermion doublers are regarded as the physical modes of system.

In this conventional formulation, the four component Dirac fermion field (16), is composed of the two low energy excitations around two different Dirac points which are spatially separated in BZ, so that the locality of the theory is not manifest. From a lattice point of view, this is quite analogous to the staggered fermion formalism in momentum space, In the next section, focusing on the analogy between the electron system of graphene and the staggered fermion formalism in lattice gauge theory, we show an alternative formulation in position space for Dirac fermion on the honeycomb lattice with manifest locality [1].

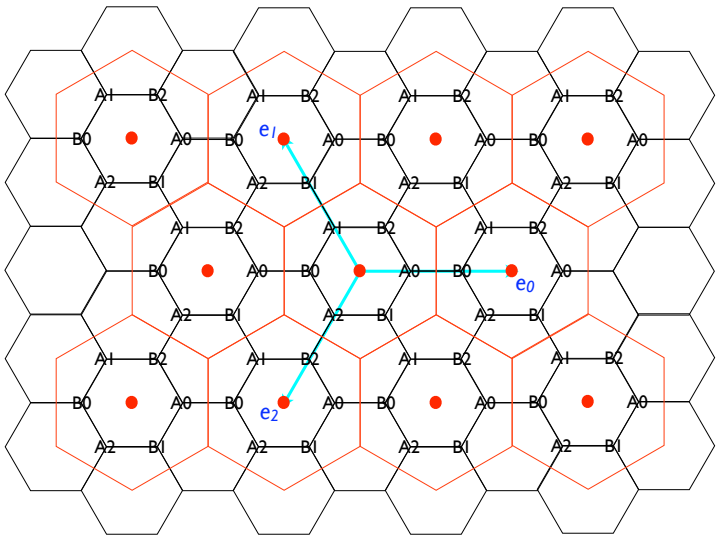

Figure 3: Fundamental lattice. The honeycomb lattice colored by red is a new fundamental lattice. The fundamental lattice involves hexagonal unit cells, and we label the vertices of each unit cell by $I\rho$ ($I = A, B; \rho = 0, 1, 2$). The red points are centers of unit cells of fundamental lattice. $\vec{e}_\rho$ ($\rho = 0, 1, 2$) colored with light blue are fundamental vectors.

3 Position space forumulation for Dirac fermion on honeycomb lattice

3.1 Reformulation of tight-binding model in position space formulation

In this section, using the idea of the staggered fermion formalism in position space [22], we present a novel formulation of tight-binding model on honeycomb lattice [1].

In the position space formulation, the d dimensional hypercubic lattice sites are relabeled. Following the experience, first of all, we introduce a new labeling of honeycomb lattice sites. As shown in Figure 3, we introduce the fundamental lattice composed of centers of hexagonal unit cells. Here, each site in the unit cell is labeled by two indices I, ρ, where I denotes sublattice degrees of freedom A, B, and ρ denotes three vertex degrees of freedom $0, 1, 2$, so that there is six internal degrees of freedom in each unit cell. The centers of hexagonal unit cells are connected by the fundamental lattice vectors given by

$$\vec{e}_0 = a\begin{pmatrix} 1, & 0 \end{pmatrix}, \quad \vec{e}_1 = a\begin{pmatrix} -1/2, & \sqrt{3}/2 \end{pmatrix}, \quad \vec{e}_2 = a\begin{pmatrix} -1/2, & -\sqrt{3}/2 \end{pmatrix}, \tag{21}$$

where, a is a lattice spacing of the fundamental lattice.

In this new site-arrangement, we define $\chi^\dagger_{I\rho}(\vec{x})$ ($\chi_{I\rho}(\vec{x})$) as the creation (annihilation) operator of quasiparticles on the fundamental lattice. The argument of the operator is the central coordinate of hexagonal unit cell of fundamental lattice. The

internal degrees of freedom associated with two indices I, ρ, is reinterpreted as spin-flavor degrees of freedom later.

Using this new labeling of field, we rewrite the tight-binding Hamiltonian at the next leading order as follows;

$$\mathcal{H} = \sum_{\vec{x},\vec{y}} \sum_{\rho,\rho'} \begin{pmatrix} \chi_{A\rho}(\vec{x}) \\ \chi_{B\rho}(\vec{x}) \end{pmatrix}^\dagger \begin{pmatrix} t'\Pi(\vec{x},\vec{y})_{\rho\rho'} & t\Phi(\vec{x},\vec{y})_{\rho\rho'} \\ t\Phi(\vec{x},\vec{y})^\dagger_{\rho\rho'} & t'\Pi(\vec{y},\vec{x})_{\rho\rho'} \end{pmatrix} \begin{pmatrix} \chi_{A\rho'}(\vec{y}) \\ \chi_{B\rho'}(\vec{y}) \end{pmatrix}, \tag{22}$$

where

$$\Phi(\vec{x},\vec{y}) = \begin{pmatrix} T_0 & 1 & 1 \\ 1 & T_1 & 1 \\ 1 & 1 & T_2 \end{pmatrix}_{\vec{x},\vec{y}}, \tag{23}$$

$$\Pi(\vec{x},\vec{y}) = \begin{pmatrix} 0 & 1+T_0+T_1^\dagger & 1+T_0+T_2^\dagger \\ 1+T_0^\dagger+T_1 & 0 & 1+T_1+T_2^\dagger \\ 1+T_0^\dagger+T_2 & 1+T_1^\dagger+T_2 & 0 \end{pmatrix}_{\vec{x},\vec{y}}, \tag{24}$$

with $(1)_{\vec{x},\vec{y}} = \delta_{\vec{x},\vec{y}}$, and $(T_\rho)_{\vec{x},\vec{y}} = \delta_{\vec{x},\vec{y}+\vec{e}_\rho}$. In Eq.(22), the off-diagonal and diagonal parts represent the nearest neighbor hopping term and next-nearest neighbor hopping term respectively, and t, t' are hopping amplitudes. The next-nearest hopping term is expressed by the nearest neighbor hopping term, and the Hamiltonian (22) is represented as follows;

$$\mathcal{H} = \sum_{\vec{x},\vec{y}} \chi(\vec{x})^\dagger \Big[tH(\vec{x},\vec{y}) + t'H^2(\vec{x},\vec{y}) - 3t' \Big] \chi(\vec{y}), \tag{25}$$

where

$$H(\vec{x},\vec{y}) = \begin{pmatrix} 0 & \Phi(\vec{x},\vec{y}) \\ \Phi(\vec{x},\vec{y})^\dagger & 0 \end{pmatrix}, \tag{26}$$

and $\chi^\dagger(\vec{x})$, $\chi(\vec{y})$ are the fermion fields with six components $\chi^\dagger_{I\rho}(\vec{x})$, $\chi(\vec{y})_{I\rho}$ ($I = A, B; \rho = 0, 1, 2$). In Eq.(25), the third term is proportional to the unit matrix, so that, in the following discussion, we omit such shift of origin of energy.

In Eq.(25), the Hamiltonian is written by 6×6 matrix $H(\vec{x},\vec{y})$ (26). Next, following the case of staggered fermion formalism, we introduce a tensor product expression for the Hamiltonian. Identifying the indices I, ρ as spin-flavor indices, we introduce the following tensor product form for an arbitrary 6×6 matrix as

$$A_{I\rho,I'\rho'} = \sum_{a=0}^{3} (\tau_a)_{I,I'} \otimes (B_a)_{\rho,\rho'}, \tag{27}$$

where τ_0 is 2×2 unit matrix, and τ_i ($i = 1, 2, 3$) are Pauli matrices, and B_a ($a = 0, 1, 2, 3$) are 3×3 Hermitian matrices. In this tensor product expression, the former acts on sublattice space $I = A, B$ (pseudospin space), while the latter acts on flavor

space $\rho = 0, 1, 2$. Using this tensor product expression, it is shown that $H(\vec{x}, \vec{y})$ is rewritten as follows [1];

$$H(\vec{x}, \vec{y}) = (\tau_1 \otimes M)\delta_{\vec{x},\vec{y}} - i\sum_{\rho}(\tau_2 \otimes \Gamma_\rho)\nabla_\rho(\vec{x}, \vec{y}) + \frac{1}{2}\sum_{\rho}(\tau_1 \otimes \Gamma_\rho)\Delta_\rho(\vec{x}, \vec{y}), \tag{28}$$

where

$$M = \begin{pmatrix} 1 & 1 & 1 \\ 1 & 1 & 1 \\ 1 & 1 & 1 \end{pmatrix}, \tag{29}$$

$$\Gamma_0 = \begin{pmatrix} 1 & 0 & 0 \\ 0 & 0 & 0 \\ 0 & 0 & 0 \end{pmatrix}, \ \Gamma_1 = \begin{pmatrix} 0 & 0 & 0 \\ 0 & 1 & 0 \\ 0 & 0 & 0 \end{pmatrix}, \ \Gamma_2 = \begin{pmatrix} 0 & 0 & 0 \\ 0 & 0 & 0 \\ 0 & 0 & 1 \end{pmatrix}. \tag{30}$$

In Eq.(28), the difference operators $\nabla_\rho(\vec{x}, \vec{y})$ and $\Delta_\rho(\vec{x}, \vec{y})$ are defined as follows;

$$\nabla_\rho(\vec{x}, \vec{y}) \equiv \frac{1}{2}[T_\rho^\dagger - T_\rho]_{\vec{x},\vec{y}}, \tag{31}$$

$$\Delta_\rho(\vec{x}, \vec{y}) \equiv \frac{1}{2}[T_\rho + T_\rho^\dagger - 2]_{\vec{x},\vec{y}}. \tag{32}$$

Substituting Eq.(28) into the Hamiltonian in Eq.(25), the tight-binding Hamiltonian in the nearest neighbor hopping approximation ($t' = 0$) reads

$$\mathcal{H} = t\sum_{\vec{x}}\chi^\dagger(\vec{x})\Big[(\tau_1 \otimes M)\chi(\vec{x}) - i\sum_{\rho}(\tau_2 \otimes \Gamma_\rho)(\nabla_\rho\chi(\vec{x})) + \frac{1}{2}\sum_{\rho}(\tau_1 \otimes \Gamma_\rho)(\Delta_\rho(\vec{x}))\Big], \tag{33}$$

where

$$\nabla_\rho\chi(\vec{x}) = \frac{1}{2}[\chi(\vec{x} + \vec{e}_\rho) - \chi(\vec{x} - \vec{e}_\rho)], \tag{34}$$

$$\Delta_\rho\chi(\vec{x}) = \frac{1}{2}[\chi(\vec{x} + \vec{e}_\rho) + \chi(\vec{x} - \vec{e}_\rho) - 2\chi(\vec{x})]. \tag{35}$$

In Eq.(33), the first term corresponds to the mass term, and the second and third term are the first and second derivative terms on the fundamental lattice. The first derivative term corresponds to the kinetic term of three flavor fermions, while the third term vanishes in the continuum limit.

The mass term, in Eq.(33), is diagonalized by the following unitary transformation

$$\chi_{I\rho}(\vec{x}) = \frac{1}{\sqrt{3}}\sum_{\rho'=0,1,2} e^{i2\pi\rho\rho'/3}\psi_{I\rho'}(\vec{x}). \tag{36}$$

Using the above transformation, the mass term is diagonalized as follows;

$$\mathcal{M} = t\sum_{\vec{x}}\psi^\dagger(\vec{x})(\tau_1 \otimes M^{diag})\psi(\vec{x}), \tag{37}$$

with

$$M^{diag} = \begin{pmatrix} 3 & 0 & 0 \\ 0 & 0 & 0 \\ 0 & 0 & 0 \end{pmatrix}. \tag{38}$$

Thus, it is shown that there appear two massless zero modes and one massive mode from the tight-binding Hamiltonian (33).

We notice that, the coefficients matrices Γ_ρ ($\rho = 0, 1, 2$) in Eq.(33) does not form Clifford algebra, so that the lattice Hamiltonian does not correspond to three flavor Dirac Hamiltonian in $(2+1)-$dimensional space-time completely. However, as we will see later, it is shown that, after integrating out the extra massive mode, the low energy effective Hamiltonian is consistent with massless Dirac Hamiltonian in the continuum limit.

3.2 Energy spectrum of tight-binding Hamiltonian

Next, we discuss the Dirac point, and physical modes from the energy spectrum analysis of the Hamiltonian (25) [1]. In momentum space, the Hamiltonian (25) is represented as

$$\mathcal{H} = \int_{BZ} \frac{d^2k}{(2\pi)^2} \tilde{\chi}^\dagger(\vec{k})[t\tilde{H}(\vec{k}) + t'\tilde{H}^2(\vec{k})]\tilde{\chi}(\vec{k}), \tag{39}$$

where $\tilde{\chi}^\dagger_{I\rho}(\vec{k})$, $\tilde{\chi}_{I\rho}(\vec{k})$ denote Fourier representations of $\chi^\dagger_{I\rho}(\vec{x})$, $\chi_{I\rho}(\vec{x})$,

$$\chi^\dagger_{I\rho}(\vec{x}) = \int_{BZ} \frac{d^2k}{(2\pi)^2} e^{-i\vec{k}\cdot\vec{x}} \tilde{\chi}^\dagger_{I\rho}(\vec{k}),\ \chi_{I\rho}(\vec{x}) = \int_{BZ} \frac{d^2k}{(2\pi)^2} e^{i\vec{k}\cdot\vec{x}} \tilde{\chi}_{I\rho}(\vec{k}), \tag{40}$$

and

$$\tilde{H}(\vec{k}) = \tau_1 \otimes M + \sum_\rho (\tau_2 \otimes \Gamma_\rho) \sin k_\rho + \sum_\rho (\tau_1 \otimes \Gamma_\rho)(\cos k_\rho - 1), \tag{41}$$

$$\begin{aligned} \tilde{H}^2(\vec{k}) = 1_{2\times 2} \otimes \Big[3M + \sum_\rho \{M, \Gamma_\rho\}(\cos k_\rho - 1) - 2\sum_\rho \Gamma_\rho(\cos k_\rho - 1) \Big] \\ + i\tau_3 \otimes \sum_\rho [M, \Gamma_\rho] \sin k_\rho, \end{aligned} \tag{42}$$

with $k_\rho = \vec{k} \cdot \vec{e}_\rho$ ($\rho = 0, 1, 2$).

3.2.1 Dirac point and physical modes

First, we consider the energy spectrum of Hamiltonian (39) at the leading order of the tight-binding approximation [1]. We set $t' = 0$ in Eq.(39), and discuss the Dirac point and physical modes.

The eigenvalue equation is given by

$$\det(\lambda \cdot 1_{6\times 6} - \tilde{H}(\vec{k})) = \lambda^6 - 9\lambda^4 - 3(z_k + z_k^* - 6)\lambda^2 - |z_k - 3|^2 = 0 \tag{43}$$

with

$$z_k = e^{-i\vec{k}\cdot\vec{e}_0} + e^{-i\vec{k}\cdot\vec{e}_1} + e^{-i\vec{k}\cdot\vec{e}_2}. \tag{44}$$

Here, the above eigenvalue equation is a cubic equation of λ^2. Thus, denoting three solutions of the cubic equation as $\phi_1^2(\vec{k})$, $\phi_2^2(\vec{k})$, $\phi_3^2(\vec{k})$, where

$$0 \leq \phi_1(\vec{k}) \leq \phi_2(\vec{k}) \leq \phi_3(\vec{k}) \leq 3, \tag{45}$$

the solution of the eigenvalue equation (43) is written as $\pm\phi_i(\vec{k})$ $(i = 1, 2, 3)$, and the energy eigenvalues of Hamiltonian (33) are given by

$$E_\pm(\phi_i) = \pm t\phi_i(\vec{k}) \ (i = 1, 2, 3). \tag{46}$$

In the half-filled electron system, the all negative eigenstates are occupied, so that the Dirac point on Fermi surface appears at zero energy level same as in the conventional formulation. From the eigenvalue equation (43), the Dirac point appears when

$$|z_k - 3| = 0. \tag{47}$$

The above condition is fulfilled only for $\vec{k} = 0$, so that, in this formulation, the Dirac point appears only at the origin of BZ.

In Figure 4, we show the dispersion relation for the quasiparticles at the leading order of the tight-binding approximation. In our formulation, the quasiparticle field has six degrees of freedom, and there appear two massless zero modes and one massive mode. From this figure, it is shown that, of the six degrees of freedom of quasiparticle field, there remains four physical degrees of freedom of two massless zero modes near the Dirac point. In the next section, we show that, after integrating out the massive mode which is unphysical near the Dirac point, the effective Hamiltonian is consistent with the conventional formulation in momentum space.

3.2.2 Effect of next-nearest neighboring term

Next, we take account of the next-nearest neighbor hopping term, and discuss the effect on the Dirac point [1].

Using $\phi_i(\vec{k})$, the energy eigenvalues of Hamiltonian at the next-leading order of the tight-binding approximation are given as follows;

$$E'_\pm(\phi_i) = \pm t\phi_i(\vec{k}) + t'\phi_i^2(\vec{k}). \tag{48}$$

In Eq.(48) if we set $t' = 0$, as mentioned above, in the half-filled electron system the Dirac point on Fermi surface appears at zero energy level since the number of positive energy eigenstates is consistent with the number of negative energy eigenstates. However, if we take account of the next-nearest neighbor hopping term, the situation becomes altered.

In order to investigate the effect, we express Eq.(48) as

$$E'_\pm(\phi_i) = t'\phi_c^2 f_\pm(|\phi_i/\phi_c|) \tag{49}$$

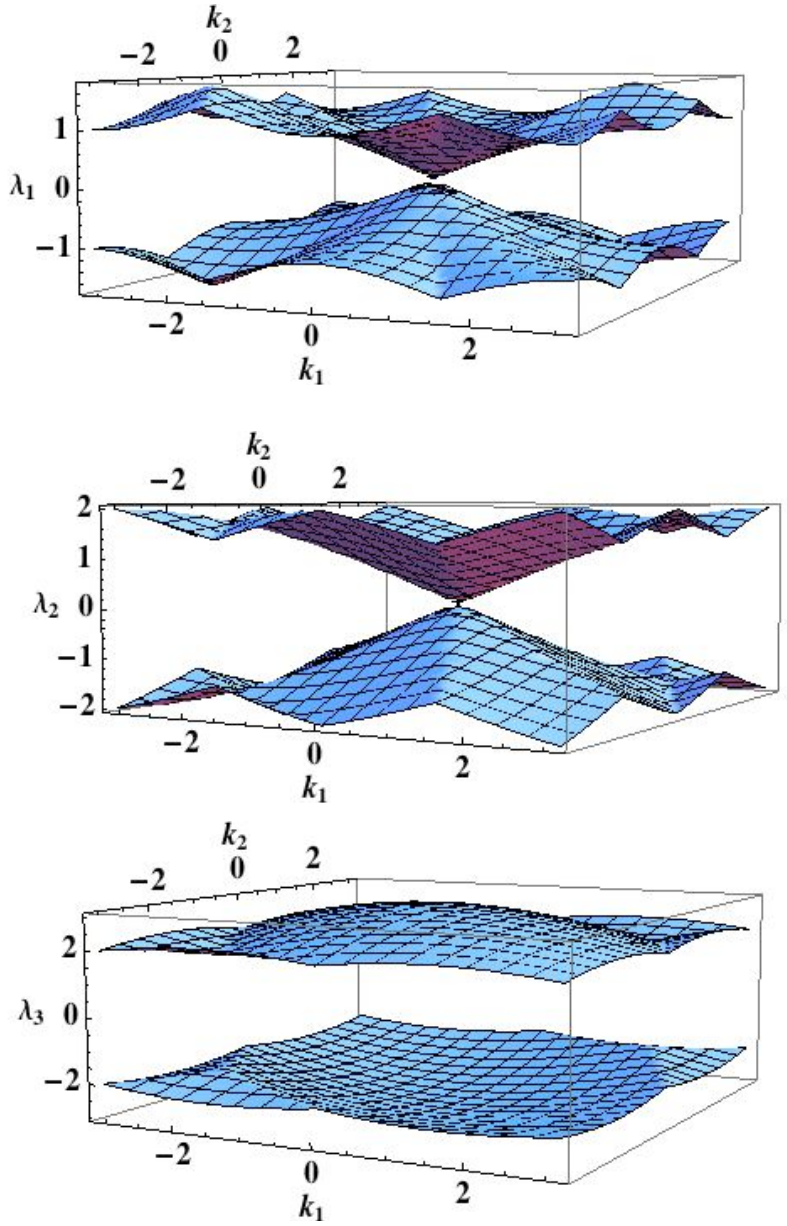

Figure 4: Dispersion relation at the leading order of the tight-binding approximation. From the top, the first, second , and third graphs show $\lambda_1 = \pm\phi_1(\vec{k})$, $\lambda_2 = \pm\phi_2(\vec{k})$, and $\lambda_3 = \pm\phi_3(\vec{k})$ respectively, where horizontal axes are $k_1 = \vec{e}_1 \cdot \vec{k}$, $k_2 = \vec{e}_2 \cdot \vec{k}$. (The source of this Figure is Fig.3 in AAM (Accepted Author Manuscript) of Ref.[1].)

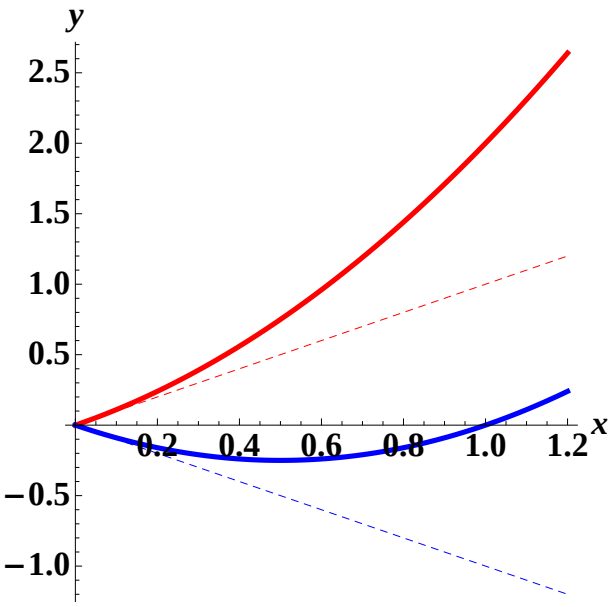

Figure 5: x axis denotes $|\phi_i/\phi_c|$, and y axis denotes energy eigenvalues divided by $t'\phi_c^2$. The dashed lines colored with red and blue are $E_+(\phi_i)/t'\phi_c^2 = |\phi_i/\phi_c|$ and $E_-(\phi_i)/t'\phi_c^2 = -|\phi_i/\phi_c|$ respectively. The solid lines colored with red and blue are $E'_+(\phi_i)/t'\phi_c^2 = f_+(|\phi_i/\phi_c|)$ and $E'_-(\phi_i)/t'\phi_c^2 = f_-(|\phi_i/\phi_c|)$. (The source of this Figure is Fig.4 in AAM (Accepted Author Manuscript) of Ref.[1].)

with $\phi_c = t/t'$ and $f_\pm(x) = x^2 \pm x$. Dividing both sides in Eq.(46), Eq.(49) by $t'\phi_c^2$, and plotting $E_\pm(\phi_i)/t'\phi_c^2$, $E'_\pm(\phi_i)/t'\phi_c^2$ as functions of $|\phi_i/\phi_c|$, we derive Figure 5. In Figure 5, we see that the eigenvalues $E'_-(\phi_i)$ remain in negative values unless ϕ_i exceeds $|\phi_c|$, while the eigenvalues $E'_+(\phi_i)$ stay in positive values at arbitrary ϕ_i. Thus, if ϕ_i does not exceed the threshold, the number of positive energy eigenstates is consistent with the negative energy eigenstates, so that, in the half-filled electron system, the Fermi surface remains in zero energy level, and the Dirac point appears only at $\vec{k} = 0$ in BZ. On the other hand, if ϕ_i exceeds the threshold, the Fermi surface no longer stays in the same energy level.

Here, the range of ϕ_i is defined as $0 \leq \phi_i \leq 3$ in Eq.(45), so that even if we consider the next-nearest neighbor hopping interaction, the Dirac point remains at the origin of BZ when $3 < \phi_c$. Especially in the graphene system, the Fermi surface does not change since $\phi_c \simeq 28$.

4 Effective theory in continuum limit

In this section, we present the derivation of the low energy effective theory from the tight-binding Hamiltonian (25), and show that, in the continuum limit, it is consistent with conventional Dirac fermion formulation in momentum space [1]. After integrating out the massive mode, the effects of the next-nearest neighbor hopping term only contributes as $\mathcal{O}(k^2)$ and $\mathcal{O}(a)$, so that here we employ the leading order of the tight-binding approximation ($t' = 0$).

In momentum space, the tight-binding Hamiltonian in the mass basis is given as follows;

$$\mathcal{H} = t\int_{BZ}\frac{d^2k}{(2\pi)^2}\tilde{\psi}^\dagger(\vec{k})[\tau_+\otimes\tilde{\Phi}'(\vec{k})+\tau_-\otimes\tilde{\Phi}'^\dagger(\vec{k})]\tilde{\psi}(\vec{k}), \tag{50}$$

where $\tilde{\psi}_{I\rho}(\vec{k})$ is the Fourier representation of $\psi_{I\rho}(\vec{x})$,

$$\psi_{I\rho}(\vec{x}) = \int_{BZ}\frac{d^2k}{(2\pi)^2}e^{i\vec{k}\cdot\vec{x}}\tilde{\psi}_{I\rho}(\vec{k}), \tag{51}$$

and

$$\tilde{\Phi}'(\vec{k}) = \frac{1}{3}\begin{pmatrix} b_0+b_1+b_2+6 & b_0+\omega^2b_1+\omega b_2 & b_0+\omega b_1+\omega^2b_2 \\ b_0+\omega b_1+\omega^2b_2 & b_0+b_1+b_2-3 & b_0+\omega^2b_1+\omega b_2 \\ b_0+\omega^2b_1+\omega b_2 & b_0+\omega b_1+\omega^2b_2 & b_0+b_1+b_2-3 \end{pmatrix} \tag{52}$$

with $b_\rho = \exp(-i\vec{k}\cdot\vec{e}_\rho)$ $(\rho = 0,1,2)$.

In order to derive the effective theory, we expand $\tilde{\Phi}'(\vec{k})$ in Eq.(50) around the Dirac point $\vec{k} = 0$ with respect to the momentum as

$$\begin{aligned}\tilde{\Phi}'(\vec{k}) &= \begin{pmatrix} 3 & 0 & 0 \\ 0 & 0 & 0 \\ 0 & 0 & 0 \end{pmatrix} - \frac{a}{2}ik_x\begin{pmatrix} 0 & 1 & 1 \\ 1 & 0 & 1 \\ 1 & 1 & 0 \end{pmatrix} - \frac{a}{2}ik_y\begin{pmatrix} 0 & -i & i \\ i & 0 & -i \\ -i & i & 0 \end{pmatrix} \\ &- \frac{a^2}{4}\begin{pmatrix} k_x^2+k_y^2 & (k_x+ik_y)^2/2 & (k_x-ik_y)^2/2 \\ (k_x-ik_y)^2/2 & k_x^2+k_y^2 & (k_x+ik_y)^2/2 \\ (k_x+ik_y)^2/2 & (k_x-ik_y)^2/2 & k_x^2+k_y^2 \end{pmatrix} + \mathcal{O}(k^3),\end{aligned} \tag{53}$$

where k_x, k_y are components of $\vec{k}$ in Cartesian coordinates, and integrate out the massive mode $\tilde{\psi}_{I0}(\vec{k})$ using its equation of motion

$$\begin{pmatrix} 0 & \tilde{\Phi}'(\vec{k})_{00} \\ \tilde{\Phi}'^\dagger(\vec{k})_{00} & 0 \end{pmatrix}\begin{pmatrix} \tilde{\psi}_{A0}(\vec{k}) \\ \tilde{\psi}_{B0}(\vec{k}) \end{pmatrix} = -\sum_{a=1,2}\begin{pmatrix} 0 & \tilde{\Phi}'(\vec{k})_{0a} \\ \tilde{\Phi}'^\dagger(\vec{k})_{0a} & 0 \end{pmatrix}\begin{pmatrix} \tilde{\psi}_{Aa}(\vec{k}) \\ \tilde{\psi}_{Ba}(\vec{k}) \end{pmatrix}. \tag{54}$$

Then, we derive the effective Hamiltonian for physical modes as follows;

$$\mathcal{H}_{\text{eff}} = v_F\int_{BZ}\frac{d^2k}{(2\pi)^2}\tilde{\psi}^\dagger(\vec{k})[H_1(\vec{k})+(a/12)H_2(\vec{k})+\mathcal{O}(\vec{k^3})]\tilde{\psi}(\vec{k}), \tag{55}$$

$$\tilde{\psi}(\vec{k}) = \begin{pmatrix} \tilde{\psi}_{A1}(\vec{k}) & \tilde{\psi}_{A2}(\vec{k}) & \tilde{\psi}_{B1}(\vec{k}) & \tilde{\psi}_{B2}(\vec{k}) \end{pmatrix}^T, \tag{56}$$

where $H_1(\vec{k})$ and $H_2(\vec{k})$ are defined as follows;

$$H_1(\vec{k}) = k_x\ (\tau_2 \otimes \sigma_1) + k_y\ (\tau_2 \otimes \sigma_2), \tag{57}$$

$$H_2(\vec{k}) = 4(k_x^2 + k_y^2)(\tau_1 \otimes 1_{2\times 2}) + (k_x^2 - k_y^2)(\tau_1 \otimes \sigma_1) - 2(k_x k_y)(\tau_1 \otimes \sigma_2). \tag{58}$$

Here, $v_F = at/2$ is the Fermi velocity, and in the above tensor product form, the former acts on sublattice space $I = A, B$, while the latter acts on flavor space $a = 1, 2$. We note that, taking the continuum limit in the above effective Hamiltonian, the higher derivative terms below $H_2(\vec{k})$ all vanish, and massless Dirac Hamiltonian with four component spinor is derived. This is consistent with the conventional Dirac fermion formulation in momentum space.

The Dirac Hamiltonian has four global symmetries generated by the following generators

$$1_{2\times 2} \otimes 1_{2\times 2},\ \tau_1 \otimes \sigma_3,\ \tau_2 \otimes 1_{2\times 2},\ \tau_3 \otimes \sigma_3, \tag{59}$$

which commute the Hamiltonian in Eq.(57). In Eq.(59), the last two generators correspond to the generators of flavor-chiral symmetries which forbid the parity invariant mass term. In our formulation [1], this mass term is defined as follows;

$$m\tilde{\psi}^\dagger(\vec{k})(\tau_1 \otimes 1_{2\times 2})\tilde{\psi}(\vec{k}). \tag{60}$$

This mass term preserves the global symmetries generated by $1_{2\times 2} \otimes 1_{2\times 2},\ \tau_1 \otimes \sigma_3$. On the other hand, this mass term breaks the global symmetries generated by $\tau_2 \otimes 1_{2\times 2}$, $\tau_3 \otimes \sigma_3$. Therefore, we identify the symmetries generated by $\tau_2 \otimes 1_{2\times 2},\ \tau_3 \otimes \sigma_3$ as flavor-chiral symmetry. In the continuum theory, these global symmetries forbid the parity invariant mass term (60).

However, at finite lattice spacing, we note that the higher derivative terms, such as $H_2(\vec{k})$ in Eq.(58), break these flavor-chiral symmetries like in the case of Wilson fermion formalism. In the next section, we consider a possibility of exact flavor-chiral symmetry deformed by lattice artifacts like in the case of overlap fermion formalism in lattice gauge theory.

We note that, in the continuum limit, the Lagarangian corresponding to the effective Hamiltonian (55) is given as follows [1];

$$\mathcal{L} = i\bar{\psi}(t, \vec{x})\Big[\partial_0\gamma_0 - v\sum_{i=1,2}\gamma_i\partial_i\Big]\psi(t, \vec{x}) \tag{61}$$

where $\bar{\psi} = \psi^\dagger\gamma_0$ and gamma matrices $\gamma_0,\ \gamma_1,\ \gamma_2$ are,

$$\gamma_0 = \begin{pmatrix} 0 & 1 \\ 1 & 0 \end{pmatrix},\ \gamma_1 = \begin{pmatrix} -i\sigma_1 & 0 \\ 0 & i\sigma_1 \end{pmatrix},\ \gamma_2 = \begin{pmatrix} -i\sigma_2 & 0 \\ 0 & i\sigma_2 \end{pmatrix}. \tag{62}$$

Apparently, these gamma matrices $\gamma_0, \gamma_1, \gamma_2$ satisfy Clifford algebra $\{\gamma_\mu, \gamma_\nu\} = 2g_{\mu\nu} \cdot 1_{4\times 4}$, where $g_{\mu\nu}$ is a metric in $(2+1)$-dimensional space-time (see Appendix A).

5 Exact symmetry on honeycomb lattice

5.1 Explicit formulation of exact symmetry

In this section, based on our formulation, we show an exact symmetry of Hamiltonian (25) even on a finite lattice [1].

Generally, there are 4 possibilities for such exact symmetry (see in Appendix B). However, we take the following ansatz for the exact symmetry;

$$\begin{aligned}\delta\chi(\vec{x}) &= i\theta[\Gamma_5]\chi(\vec{x}) \\ &= i\theta\Big[(\tau_3\otimes X)\chi(\vec{x}) + \frac{1}{2}\sum_\rho(\tau_3\otimes Y_\rho)(\Delta_\rho\chi(\vec{x}) + 2\chi(\vec{x})) + \frac{1}{i}\sum_\rho(1\otimes Z_\rho)(\nabla_\rho\chi(\vec{x}))\Big],\end{aligned} \tag{63}$$

where X, Y_ρ, and Z_ρ ($\rho = 0, 1, 2$) are undetermined 3×3 Hermitian matrices. In the above equation, the first and second derivative terms correspond to $\mathcal{O}(a)$ terms, and Γ_5 is expected to conform to the global flavor-chiral symmetry generated by $\tau_3\otimes\sigma_3$ in the continuum limit.

In order to determine the coefficient matrices X, Y_ρ, and Z_ρ, we perform the Fourier transformation of $\chi(\vec{x})$, $\chi^\dagger(\vec{x})$, and then impose $[\tilde{H}, \tilde{\Gamma}_5] = 0$ on $\tilde{\Gamma}_5$ which is a Fourier representation of Γ_5 in Eq.(63). From this condition, we derive a system of equations for X, Y_ρ, and Z_ρ (see in Appendix C). Solving the equations, we derive the following unique solution for X, Y_ρ, and Z_ρ ($\rho = 0, 1, 2$);

$$X = \begin{pmatrix} 0 & -i & i \\ i & 0 & -i \\ -i & i & 0 \end{pmatrix}, \tag{64}$$

$$Y_0 = \begin{pmatrix} 0 & -i & i \\ i & 0 & 0 \\ -i & 0 & 0 \end{pmatrix},\ Y_1 = \begin{pmatrix} 0 & -i & 0 \\ i & 0 & -i \\ 0 & i & 0 \end{pmatrix},\ Y_2 = \begin{pmatrix} 0 & 0 & i \\ 0 & 0 & -i \\ -i & i & 0 \end{pmatrix}, \tag{65}$$

$$Z_0 = \begin{pmatrix} 0 & -1 & 1 \\ -1 & 0 & 0 \\ 1 & 0 & 0 \end{pmatrix},\ Z_1 = \begin{pmatrix} 0 & 1 & 0 \\ 1 & 0 & -1 \\ 0 & -1 & 0 \end{pmatrix},\ Z_2 = \begin{pmatrix} 0 & 0 & -1 \\ 0 & 0 & 1 \\ -1 & 1 & 0 \end{pmatrix}. \tag{66}$$

Here, if we represent Eq.(63) in terms of $\chi_{A\rho}(\vec{x})$, $\chi_{B\rho}(\vec{x})$, the above exact symmetry is represented as follows;

$$\begin{aligned}\delta\chi_{A\rho}(\vec{x}) &= \theta[\chi_{A_{\rho+1}}(\vec{x}+\vec{e}_{\rho+1}) - \chi_{A_{\rho-1}}(\vec{x}-\vec{e}_\rho) \\ &\quad +\chi_{A_{\rho+1}}(\vec{x}-\vec{e}_\rho) - \chi_{A_{\rho-1}}(\vec{x}+\vec{e}_{\rho-1}) + \chi_{A_{\rho+1}}(\vec{x}) - \chi_{A_{\rho-1}}(\vec{x})], \qquad (67) \\ \delta\chi_{B\rho}(\vec{x}) &= \theta[-\chi_{B_{\rho+1}}(\vec{x}-\vec{e}_{\rho+1}) + \chi_{B_{\rho-1}}(\vec{x}+\vec{e}_\rho) \\ &\quad -\chi_{B_{\rho+1}}(\vec{x}+\vec{e}_\rho) + \chi_{B_{\rho-1}}(\vec{x}-\vec{e}_{\rho-1}) - \chi_{B_{\rho+1}}(\vec{x}) + \chi_{B_{\rho-1}}(\vec{x})]. \qquad (68)\end{aligned}$$

Eqs.(67), (68) show that the exact symmetry Eq.(63) includes only the next-nearest neighbor sites (see Figure 6), and, if we take the conventional labeling of quasiparticle

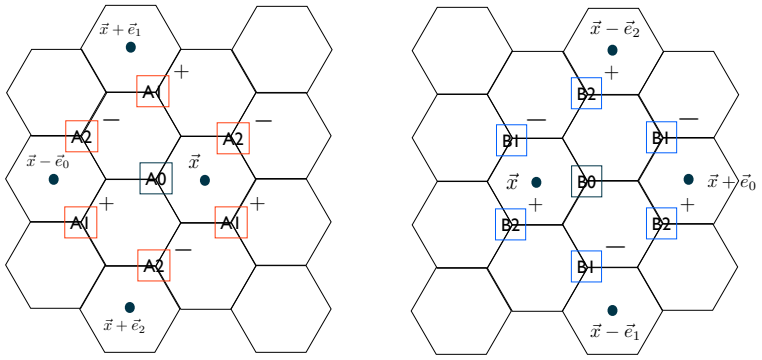

Figure 6: Geometrical picture of Eq.(67), (68). Left and right panels show the transformation for $\chi_{A0}(\vec{x})$ and one for $\chi_{B0}(\vec{x})$ respectively. The transformation for $\chi_{A0}(\vec{x})$ ($\chi_{B0}(\vec{x})$) involves $\chi_{A\rho}(\vec{x})$ ($\chi_{B\rho}(\vec{x})$) surrounded by red (blue) square, where sign denotes its overall factor. (The source of this Figure is Fig.5 in AAM (Accepted Author Manuscript) of Ref.[1].)

fields $a(\vec{x})$, $b(\vec{x})$, the exact symmetry (63) is also represented as follows;

$$\begin{aligned}\delta a(\vec{x}) = \theta[&a(\vec{x}+\vec{s}_2-\vec{s}_3)-a(\vec{x}-\vec{s}_1+\vec{s}_2)+a(\vec{x}+\vec{s}_3-\vec{s}_1)\\ &-a(\vec{x}-\vec{s}_2+\vec{s}_3)+a(\vec{x}+\vec{s}_1-\vec{s}_2)-a(\vec{x}-\vec{s}_3+\vec{s}_1)] \qquad (69)\\ \delta b(\vec{x}) = \theta[&b(\vec{x}+\vec{s}_2-\vec{s}_3)-b(\vec{x}-\vec{s}_1+\vec{s}_2)+b(\vec{x}+\vec{s}_3-\vec{s}_1)\\ &-b(\vec{x}-\vec{s}_2+\vec{s}_3)+b(\vec{x}+\vec{s}_1-\vec{s}_2)-b(\vec{x}-\vec{s}_3+\vec{s}_1)] \qquad (70)\end{aligned}$$

In Eq.(63), if we take the continuum limit $a \to 0$, the transformation (63) becomes

$$\delta\chi(\vec{x}) = i\theta\Big[\tau_3 \otimes (X + \sum_\rho Y_\rho)\Big]\chi(\vec{x}) = 3i\theta[\tau_3 \otimes X]\chi(\vec{x}). \qquad (71)$$

In the mass basis, X is transformed to the following form,

$$\begin{pmatrix} 0 & 0 & 0 \\ 0 & 1 & 0 \\ 0 & 0 & -1 \end{pmatrix}, \qquad (72)$$

except for the overall factor. Thus, in the continuum limit, the exact symmetry conforms to the global flavor-chiral symmetry generated by $\tau_3 \otimes \sigma_3$.

We note that the exact symmetry can explain the gapless nature of non-interacting graphene system. Under the parity symmetry, Z_3 symmetry, the time reversal symmetry, as well as the exact $U(1)$ symmetry, it is shown that the gapless modes should appear in the monolayer graphene system [33]. In the next section, we present the explanation.

5.2 Gapless modes in monolayer graphene

In this section, we show that the gaplessness in the non-interacting monolayer graphene system can be explained from the parity symmetry, Z_3 symmetry, the time reversal symmetry, as well as the exact $U(1)$ symmetry [33].

To achieve this, we consider the Hamiltonian of constant mode. In the limit $k_\rho \to 0$, the Hamiltonian of constant mode is generally written as the following form;

$$\mathcal{H}_{low} = \tilde{\chi}^\dagger \Big[(1_{2\times 2} \otimes F) + (\tau_1 \otimes C_1) + (\tau_2 \otimes C_2) + (\tau_3 \otimes C_3) \Big] \tilde{\chi}, \tag{73}$$

where $\tilde{\chi}$ denotes the constant mode of $\tilde{\chi}(\vec{k})$, and F, C_i $(i = 1, 2, 3)$ are arbitrary 3×3 Hermitian matrices. Under the Z_3 symmetry, F, and C_i $(i = 1, 2, 3)$ take the following forms;

$$F = \begin{pmatrix} c & c+if & c-if \\ c-if & c & c+if \\ c+if & c-if & c \end{pmatrix}, \; C_i = \begin{pmatrix} c_i & q_i & q_i^* \\ q_i^* & c_i & q_i \\ q_i & q_i^* & c_i \end{pmatrix}, \tag{74}$$

where c, f, c_i $(i = 1, 2, 3)$ are arbitrary real numbers, and q_i is an arbitrary complex number. Furthermore, if we impose the parity symmetry, the time reversal symmetry as well as the global exact symmetry on the Hamiltonian $\mathcal{H}_{\rm low}$ in Eq.(73) [b], it should be the following form;

$$\mathcal{H}_{low} = \tilde{\chi}^\dagger \Big[c(1_{2\times 2} \otimes M) + c_1(\tau_1 \otimes M) \Big] \tilde{\chi}, \tag{79}$$

with

$$M = \begin{pmatrix} 1 & 1 & 1 \\ 1 & 1 & 1 \\ 1 & 1 & 1 \end{pmatrix}. \tag{80}$$

Here, Eq.(79) can be easily diagonalized by the unitary transformation (36) as follows;

$$\mathcal{H}_{low} = \tilde{\psi}^\dagger \Big[c(1_{2\times 2} \otimes M^{diag}) + c_1(\tau_1 \otimes M^{diag}) \Big] \tilde{\psi}, \tag{81}$$

[b] The parity symmetry and time reversal symmetry on the Hamiltonian $\mathcal{K}$ are represented in this formulation as follows;

$$(\tau_1 \otimes 1_{3\times 3}) \tilde{K}(\vec{k}) (\tau_1 \otimes 1_{3\times 3}) = \tilde{K}(-\vec{k}) \tag{75}$$

$$\tilde{K}^*(\vec{k}) = \tilde{K}(-\vec{k}), \tag{76}$$

where $\tilde{K}(\vec{k})$ is defined in

$$\mathcal{K} = \int \frac{d^2k}{(2\pi)^2} \tilde{\chi}(\vec{k}) [\tilde{K}(\vec{k})] \tilde{\chi}(\vec{k}). \tag{77}$$

The transformation of the exact symmetry for constant mode $\tilde{\chi}$ is generated by $\tau_3 \otimes X$, where

$$X = \begin{pmatrix} 0 & -i & i \\ i & 0 & -i \\ -i & i & 0 \end{pmatrix}. \tag{78}$$

where $\tilde{\psi}$ denotes the constant mode of $\tilde{\psi}(\vec{k})$, and M^{diag} is given as

$$M^{diag} = \begin{pmatrix} 3 & 0 & 0 \\ 0 & 0 & 0 \\ 0 & 0 & 0 \end{pmatrix}. \tag{82}$$

Thus, it is shown that the gapless modes should appear in the system.

In condensed matter physics, the gaplessness in the monolayer graphene system is conventionally understood by the inversion and C_3 symmetries [12, 13]. The exact symmetry presented here gives another explanation for the gaplessness in the monolayer graphene system, while it is a future task to study whether our symmetry is related to those symmetries or not.

In the next section, we present an extension of our formulation to the AB-stacked bilayer graphene system [33]. In the experiments, gapless modes are also observed in bilayer graphene, armchair/zigzag graphene nano ribbons, and non-chiral carbon nanotubes. Our formulation may be useful to understand those gapless modes.

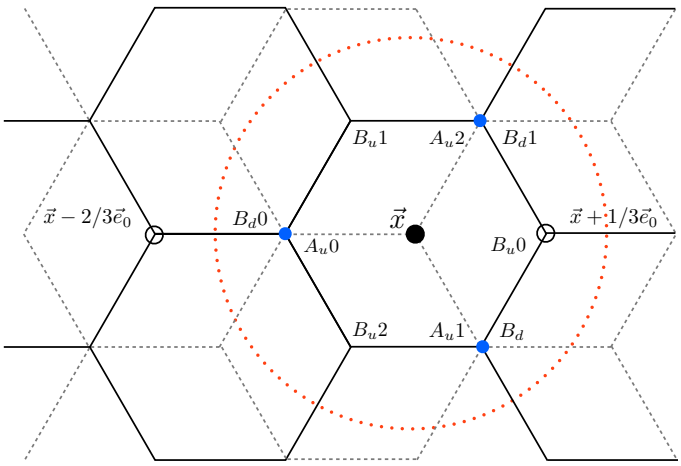

Figure 7: Lattice structure of bilayer graphene (viewed from the above). Two honeycomb lattice sheets presented in black solid and gray dashed lines are upper and lower layer in AB-stacked bilayer graphene. The black and white circles denote the centers of the unit cells of that fundamental lattice, which are introduced in the monolayer graphene system. The six vertices of hexagonal unit cell in upper and lower layers are labeled as $I_u\rho$ and $I_d\rho$ $(I = A, B; \rho = 0, 1, 2)$ respectively. The blue circles denote the points where A sites in upper layer and B sites in lower layer overlap.

6 Exact symmetry of bilayer graphene

In this section, we present the extension of the position space formulation to the AB-stacked bilayer graphene system, as well as the formulation of exact symmetry [33].

The Figure 7 shows how two honeycomb lattice sheets are stacked in the position space formulation. Here, the layers are shifted by $1/3\vec{e}_0$ (or $1/3\vec{e}_1$, $1/3\vec{e}_2$) in the plane, and the distance between two layers is given as 3.34 $\mathring{A}$ [34].

In Figure 7, the leading order of interlayer hopping interaction between two layers occurs at the points colored with blue. Thus, defining the creation (annihilation) operators on upper and lower layer as $\chi^\dagger_{u,I\rho}(\vec{x})(\chi_{u,I\rho}(\vec{x}))$, $\chi^\dagger_{d,I\rho}(\vec{x})(\chi_{d,I\rho}(\vec{x}))$, where the indices u, d denote upper and lower layer respectively, the tight binding Hamiltonian of AB-stacked bilayer graphene is given as follows;

$$\begin{aligned}\mathcal{H}_B = \; & - \; t\sum_{l=u,d}\sum_{\vec{x}}\chi^\dagger_l(\vec{x})\Big[(\tau_1\otimes M)\chi_l(\vec{x}) - i\sum_\rho(\tau_2\otimes\Gamma_\rho)(\nabla_\rho\chi_l(\vec{x})) \\ & + \; \frac{1}{2}\sum_\rho(\tau_1\otimes\Gamma_\rho)(\Delta_\rho\chi_l(\vec{x}))\Big] \\ & - \; \gamma\sum_{\vec{x}}\chi^\dagger_u(\vec{x})\Big[(\tau_+\otimes\Gamma_0)\chi_d(\vec{x}-2/3\vec{e}_0) + (\tau_+\otimes V)\chi_d(\vec{x}+1/3\vec{e}_0) + h.c.\Big],\end{aligned} \tag{83}$$

where

$$V = \begin{pmatrix} 0 & 0 & 0 \\ 0 & 0 & 1 \\ 0 & 1 & 0 \end{pmatrix}. \tag{84}$$

In Eq.(83), the first and second lines are the nearest neighbor hopping term in each layer, and the third line is the leading order of interlayer hopping interaction between two layers. t, γ are hopping amplitudes. We note that, in the AB-stacked bilayer graphene system, $t \simeq 3$ eV, and $\gamma \simeq 0.4$ eV [35].

In Eq.(83), if we neglect the interlayer hopping term and set $\gamma = 0$, the Hamiltonian is invariant under the following infinitesimal transformations for $\chi_u(\vec{x})$, $\chi_d(\vec{x})$ as

$$\delta\chi_u(\vec{x}) = i\theta\Big[(\tau_3 \otimes X)\chi_u(\vec{x}) + \frac{1}{2}\sum_\rho (\tau_3 \otimes Y_\rho)(\Delta_\rho \chi_u(\vec{x}) + 2\chi_u(\vec{x})) + \frac{1}{i}\sum_\rho (1 \otimes Z_\rho)(\nabla_\rho \chi_u(\vec{x}))\Big], \tag{85}$$

$$\delta\chi_d(\vec{x}) = i\theta'\Big[(\tau_3 \otimes X)\chi_d(\vec{x}) + \frac{1}{2}\sum_\rho (\tau_3 \otimes Y_\rho)(\Delta_\rho \chi_d(\vec{x}) + 2\chi_d(\vec{x})) + \frac{1}{i}\sum_\rho (1 \otimes Z_\rho)(\nabla_\rho \chi_d(\vec{x}))\Big], \tag{86}$$

where the coefficients matrices X, Y_ρ, Z_ρ $(\rho = 0, 1, 2)$ are same as in monolayer, and given as

$$X = \begin{pmatrix} 0 & -i & i \\ i & 0 & -i \\ -i & i & 0 \end{pmatrix}, \tag{87}$$

$$Y_0 = \begin{pmatrix} 0 & -i & i \\ i & 0 & 0 \\ -i & 0 & 0 \end{pmatrix},\ Y_1 = \begin{pmatrix} 0 & -i & 0 \\ i & 0 & -i \\ 0 & i & 0 \end{pmatrix},\ Y_2 = \begin{pmatrix} 0 & 0 & i \\ 0 & 0 & -i \\ -i & i & 0 \end{pmatrix}, \tag{88}$$

$$Z_0 = \begin{pmatrix} 0 & -1 & 1 \\ -1 & 0 & 0 \\ 1 & 0 & 0 \end{pmatrix},\ Z_1 = \begin{pmatrix} 0 & 1 & 0 \\ 1 & 0 & -1 \\ 0 & -1 & 0 \end{pmatrix},\ Z_2 = \begin{pmatrix} 0 & 0 & -1 \\ 0 & 0 & 1 \\ -1 & 1 & 0 \end{pmatrix}. \tag{89}$$

However, we note that even if we take account of the interlayer hopping interaction in Eq.(83), it is shown that the Hamiltonian $\mathcal{H}_B$ is invariant under the above transformation with $\theta = \theta'$, so that the symmetry remains exact. The details of calculation is given in Appendix D.

7 Summary and discussion

In this thesis, we showed the novel formulation for the construction of Dirac fermion formulation on honeycomb lattice in position space, which could be regarded as the counterpart of the conventional formulation in momentum space, as well as the explicit formulation of exact symmetry on honeycomb lattice [1]. Besides, we extended this formulation to the AB-stacked bilayer graphene system [33].

In this formulation, we first considered the new labelling of degrees of freedom of the honeycomb lattice sites, and introduced the quasiparticle field defined on the fundamental lattice with hexagonal unit cells. In this site-arrangement, the honeycomb lattice sites were labelled by a center coordinate of unit cell, and indices I, ρ in a unit cell. Using this relabelling of field, we reformulated the tight-binding Hamiltonian, and showed that the Hamiltonian was constructed by kinetic term and second derivative term, which were written in the tensor product form associated with A, B sublattice and three vertex degrees of freedom in a hexagonal unit cell, and besides there appeared two massless zero modes and one massive mode.

In this formulation, it was shown that the Dirac point appeared only at the origin of BZ, and was stable to the next nearest neighbor hopping interaction. From the analysis of energy spectrum, it was also shown that, of the six degrees of freedom of quasiparticle field, there remained four physical degrees of freedom of two massless zero modes near the Dirac point. In the derivation of the effective theory, we integrated out the massive mode, which was unphysical near the Dirac point, and showed that, in the continuum limit, the effective theory was consistent with the conventional formulation in momentum space.

We found an exact $U(1)$ symmetry at finite lattice spacing, which protected the masslessness of Dirac fermion, and showed that the symmetry remained exact even if we considered the interlayer hopping interaction in bilayer graphene system. We showed that our new $U(1)$ symmetry could play a crucial role in preserving the gaplessness in monolayer graphene. Although conventionally the gaplessness is understood by discrete symmetries, i.e. the inversion and C_3 symmetries, whether these discrete symmetries are related to our $U(1)$ symmetry or not is an open problem. This is a subject which should be studied further.

This formulation may be useful for studying some non-perturbative dynamics in condensed matter physics such as spontaneous chiral symmetry breaking in suspended graphene [7, 25, 26, 27, 28, 29], while, in a point of view of lattice gauge theory, our formulation can also be regarded as one of the lattice fermion formalisms on two dimensional space lattice.

In lattice gauge theory, as is well known, there is the fermion doubling problem to define massless Dirac fermion on the lattice, and it is needed to present a formalism which does not conflict the doubling problem, and enables a faster numerical simulation for studying non-perturbative dynamics in quantum field theory. To achieve this, in some literature, it has been studied to extend the lattice structure to non-hypercubic lattices. For instance, in Ref.[30], a new lattice fermion formalism on four dimensional hyperdiamond lattice was proposed as an extension of the graphene model on the honeycomb lattice. This regularization method has some advantages for studying

non-perturbative dynamics in quantum field theory. However, it seems possible to present another extensions in more general forms. Our formulation will be a first step for such study, and may be widely useful for studying other lattice regularization methods on non-hypercubic lattices.

Acknowledgments

I would like to greatly thank my supervisor Tetsuya Onogi for his fruitful advise, discussion. I am also very grateful to Yutaka Hosotani, Hidenori Fukaya, and Satoshi Yamaguchi, for useful discussion, comments, and various supports. I would like to appreciate Keiko Takeda for her various supports. Finally, I thank all members of particle physics theory group at Osaka University.

A Model in Lagrange formulation

Here, the model in Lagrange formulation is explained [1]. If we add a mass term to the effective theory, Hamiltonian is written as follows;

$$\mathcal{H} = \int \frac{d^2k}{(2\pi)^2} \tilde{\psi}^\dagger(\vec{k})[\alpha_1 k_1 + \alpha_2 k_2 + m\beta]\tilde{\psi}(\vec{k}), \tag{90}$$

where

$$\alpha_1 = \begin{pmatrix} 0 & -i\sigma_1 \\ i\sigma_1 & 0 \end{pmatrix}, \quad \alpha_2 = \begin{pmatrix} 0 & -i\sigma_2 \\ i\sigma_2 & 0 \end{pmatrix}. \tag{91}$$

β is a Hermitian matrix and we may take following choices;

$$\begin{pmatrix} 0 & 1 \\ 1 & 0 \end{pmatrix}, \begin{pmatrix} 1 & 0 \\ 0 & -1 \end{pmatrix}. \tag{92}$$

Here the first gives parity even mass term while the second gives parity odd mass term. However the parity odd mass term is forbidden by parity symmetry, thus we choose the parity even mass term here. Then transforming above Hamiltonian to Lagrangian in real space, we obtain the following Dirac Lagrangian.

$$\mathcal{L} = i\psi^\dagger(t,\vec{x})\Big[\partial_0 + v\sum_{i=1,2}\alpha_i\partial_i - m\beta\Big]\psi(t,\vec{x}) \tag{93}$$

$$= i\bar{\psi}(t,\vec{x})\Big[\partial_0\gamma_0 - v\sum_{i=1,2}\gamma_i\partial_i - m\Big]\psi(t,\vec{x}) \tag{94}$$

where $\bar{\psi} = \psi^\dagger\beta$ and $\gamma_0 = \beta,\ \gamma_1 = -\beta\alpha_1,\ \gamma_2 = -\beta\alpha_2$. Evidently, the gamma matrices $\gamma_0, \gamma_1, \gamma_2$ satisfy Clifford algebra $\{\gamma_\mu, \gamma_\nu\} = 2g_{\mu\nu}\cdot 1_{4\times4}$, where $g_{\mu\nu}$ is a metric in $(2+1)$-dimensional space-time.

B Possibilities for exact symmetry

In general, there are 4 candidates for an exact symmetry Γ_5, involving $\mathcal{O}(a)$ lattice artifacts as follows;

$$1_{2\times2}\otimes A_5 + \mathcal{O}(a),\ \tau_1\otimes B_5 + \mathcal{O}(a),\ \tau_2\otimes C_5 + \mathcal{O}(a),\ \tau_3\otimes D_5 + \mathcal{O}(a), \tag{95}$$

where A_5, B_5, C_5, D_5 are 3×3 Hermitian matrices. Since Γ_5 involves $\mathcal{O}(a)$ lattice artifacts, in the Fourier representation, such transformation is momentum dependent and written as

$$\delta\tilde{\chi}(\vec{k}) = i\theta\tilde{\Gamma}_5(\vec{k})\tilde{\chi}(\vec{k}), \tag{96}$$

where $\tilde{\Gamma}_5(\vec{k})$ is the Fourier representation of Γ_5. In order to derive an exact symmetry, we expand $\tilde{\Gamma}_5(\vec{k})$ with respect to k, and consider to determine the expansion coefficients

by imposing $[\tilde{H}(\vec{k}), \tilde{\Gamma}_5(\vec{k})] = 0$ on $\tilde{\Gamma}_5(\vec{k})$ order by order. The Taylor expansion of $\tilde{\Gamma}_5(\vec{k})$ around $k = 0$ with respect to k is written as follows;

$$\begin{aligned}\tilde{\Gamma}_5(\vec{k}) &= \tilde{\Gamma}_5 + (\tilde{\Gamma}_{5k}k + \tilde{\Gamma}^\dagger_{5k}k^*) - \frac{1}{2}(\tilde{\Gamma}_{5kk}k^2 + \tilde{\Gamma}^\dagger_{5kk}k^2 + \tilde{\Gamma}_{5kk^*}kk^*) \\ &- \frac{1}{6}(\tilde{\Gamma}_{5kkk}k^3 + \tilde{\Gamma}^\dagger_{5kkk}k^{*3} + 3\tilde{\Gamma}_{5kkk^*}k^2k^* + 3\tilde{\Gamma}^\dagger_{5kkk^*}kk^{*2}) + \cdots, \end{aligned} \tag{97}$$

where k is defined as $k = (k_x + ik_y)/2$, and $\tilde{\Gamma}_5$, $\tilde{\Gamma}_{5kk^*}$ are 6×6 Hermitian matrices, and $\tilde{\Gamma}_{5k}$, $\tilde{\Gamma}_{5kkk}$, $\tilde{\Gamma}_{5kkk^*}$ are 6×6 complex matrices. Here, the coefficients matrices of momentum expansion are determined order by order from the condition $[\tilde{H}(\vec{k}), \tilde{\Gamma}_5(\vec{k})] = 0$.

For instance, if we consider the case of $\tau_3 \otimes D + \mathcal{O}(a)$ in Eq.(95), which is expected to conform to the global flavor-chiral symmetry generated by $\tau_3 \otimes \sigma_3$ in the continuum limit, it is shown that, at the third order of momentum expansion, the coefficients in Eq.(97) should satisfy the following equations;

$$\tilde{\Gamma}_5 = \tau_3 \otimes D_5, \tag{98}$$
$$\tilde{\Gamma}_{5k} = 1_{2\times2} \otimes D_{5k}, \tag{99}$$
$$\tilde{\Gamma}_{5kk} = \tau_3 \otimes D_{5kk},\ \tilde{\Gamma}_{5kk^*} = \tau_3 \otimes D_{5kk^*}, \tag{100}$$
$$\tilde{\Gamma}_{5kkk} = 1_{2\times2} \otimes D_{5kkk},\ \tilde{\Gamma}_{5kkk^*} = 1_{2\times2} \otimes D_{5kkk^*}, \tag{101}$$
$$\{M, D_5\} = 0, \tag{102}$$
$$\{\Omega^\dagger, D_5\} + [M, D_{5k}] = 0 \tag{103}$$
$$i\{M, D_{5kk}\} + i\{\Omega, D_5\} + 2[\Omega^\dagger, D_{5k}] = 0 \tag{104}$$
$$2iD_5 + i\{M, D_{5kk^*}+\}[\Omega, D_{5k}] + [\Omega^\dagger, D^\dagger_{5k}] = 0, \tag{105}$$
$$2iD_5 + 3i\{\Omega^\dagger, D_{5kk}\} + 3[\Omega, D_{5k}] + [M, D_{5kkk}] = 0, \tag{106}$$
$$\begin{aligned} &i\{\Omega^\dagger, D_5\} + i\{\Omega, D_{5kk}\} + 2i\{\Omega^\dagger, D_{5kk^*}\} + [\Omega, D_{5k^*}] \\ &+[M, D_{5kkk^*}] = 0, \end{aligned} \tag{107}$$

where D_5, D_{5kk^*} are 3×3 Hermitian matrices, and D_{5k}, D_{5kk}, D_{5kkk}, D_{5kkk^*} are 3×3 complex matrices, and Ω is defined as

$$\Omega = \begin{pmatrix} 1 & 0 & 0 \\ 0 & \omega & 0 \\ 0 & 0 & \omega^2 \end{pmatrix}. \tag{108}$$

In this way, we considered the all candidates in Eq.(95). In the result, it was found that $\tau_1 \otimes B + \mathcal{O}(a)$, and $\tau_2 \otimes C + \mathcal{O}(a)$ were denied, while $1_{2\times2} \otimes A + \mathcal{O}(a)$, and $\tau_3 \otimes D + \mathcal{O}(a)$ were fine at the third order of expansion. Following the result, in section 5, we take the following ansatz for the exact symmetry as

$$\begin{aligned}\delta\chi(\vec{x}) = i\theta\Big[&(\tau_3 \otimes X)\chi(\vec{x}) + \frac{1}{2}\sum_\rho(\tau_3 \otimes Y_\rho)(\Delta_\rho\chi(\vec{x}) + 2\chi(\vec{x})) \\ &+\frac{1}{i}\sum_\rho(1 \otimes Z_\rho)(\nabla_\rho\chi(\vec{x}))\Big]. \end{aligned} \tag{109}$$

C Derivation of exact symmetry

Here, we show the derivation of exact symmetry [1]. In order to determine X, Y_ρ, and Z_ρ, we take the Fourier representations of $\chi(\vec{x}), \chi^\dagger(\vec{x})$. In momentum space, the Hamiltonian at the leading order of tight-binding approximation is represented as follows;

$$\mathcal{H} = \int \frac{d^2k}{(2\pi)^2} \tilde{\chi}^\dagger(\vec{k}) \Big[(\tau_1 \otimes \Lambda) + \sum_\rho e^{ik_\rho} (\tau_- \otimes \Gamma_\rho) + \sum_\rho e^{-ik_\rho} (\tau_+ \otimes \Gamma_\rho) \Big] \tilde{\chi}(\vec{k}) \quad (110)$$

with $\tau_\pm \equiv (\tau_1 \pm i\tau_2)/2$ and $\Lambda \equiv M - 1$. Besides, $\tilde{\Gamma}_5(\vec{k})$ is also represented as follows;

$$\tilde{\Gamma}_5(\vec{k}) = (\tau_3 \otimes X) + \sum_\rho e^{ik_\rho} \gamma_\rho + \sum_\rho e^{-ik_\rho} \gamma_\rho^\dagger, \quad (111)$$

where

$$\gamma_\rho = \frac{\tau_3 + 1}{2} \otimes W_\rho^\dagger + \frac{\tau_3 - 1}{2} \otimes W_\rho, \quad (112)$$

with $W_\rho = \frac{1}{2}(Y_\rho + iZ_\rho)$.

Then, imposing $[\tilde{H}(\vec{k}), \tilde{\Gamma}_5(\vec{k})] = 0$ on $\tilde{\Gamma}_5(\vec{k})$, we obtain the following equations;

$$\{\Lambda, X\} + \sum_\rho (\Gamma_\rho W_\rho + W_\rho^\dagger \Gamma_\rho) = 0 \quad (113)$$

$$\{\Gamma_\rho, X\} + \Lambda W_\rho^\dagger + W_\rho \Lambda = 0 \quad (114)$$

$$\Lambda W_\rho + W_\rho^\dagger \Lambda + \sum_{\sigma \neq \lambda (\sigma, \lambda \neq \rho)} (\Gamma_\sigma W_\lambda^\dagger + W_\lambda \Gamma_\sigma) = 0 \quad (115)$$

$$\Gamma_\rho W_\rho^\dagger + W_\rho \Gamma_\rho = 0 \quad (116)$$

$$\Gamma_\rho W_\sigma + W_\sigma^\dagger \Gamma_\rho = 0 \ (\rho \neq \sigma). \quad (117)$$

Solving these equation for X and $W_\rho (\rho = 0, 1, 2)$, the unique solution is found as follows;

$$X = \begin{pmatrix} 0 & -i & i \\ i & 0 & -i \\ -i & i & 0 \end{pmatrix}, \quad (118)$$

$$W_0 = \begin{pmatrix} 0 & -i & i \\ 0 & 0 & 0 \\ 0 & 0 & 0 \end{pmatrix}, \ W_1 = \begin{pmatrix} 0 & 0 & 0 \\ i & 0 & -i \\ 0 & 0 & 0 \end{pmatrix}, \ W_2 = \begin{pmatrix} 0 & 0 & 0 \\ 0 & 0 & 0 \\ -i & i & 0 \end{pmatrix}, \quad (119)$$

The coefficients matrices Y_ρ, Z_ρ are determined by $Y_\rho = W_\rho + W_\rho^\dagger$, $Z_\rho = (W_\rho - W_\rho^\dagger)/i$ respectively.

D Derivation of exact symmetry in bilayer graphene

Here, we show the derivation of exact symmetry in bilayer graphene [33]. The infinitesimal transformations of exact symmetry for $\chi_l(\vec{x})$ $(l = u, d)$ are written as follows;

$$\delta\chi_u(\vec{x}) = i\theta\Big[(\tau_3 \otimes X)\chi_u(\vec{x}) + \frac{1}{2}\sum_\rho(\tau_3 \otimes Y_\rho)(\Delta_\rho\chi_u(\vec{x}) + 2\chi_u(\vec{x})) + \frac{1}{i}\sum_\rho(1 \otimes Z_\rho)(\nabla_\rho\chi_u(\vec{x}))\Big], \tag{120}$$

$$\delta\chi_d(\vec{x}) = i\theta\Big[(\tau_3 \otimes X)\chi_d(\vec{x}) + \frac{1}{2}\sum_\rho(\tau_3 \otimes Y_\rho)(\Delta_\rho\chi_d(\vec{x}) + 2\chi_d(\vec{x})) + \frac{1}{i}\sum_\rho(1 \otimes Z_\rho)(\nabla_\rho\chi_d(\vec{x}))\Big], \tag{121}$$

where the coefficients matrices X, Y_ρ, Z_ρ, $(\rho = 0, 1, 2)$ are 6×6 Hermitian matrices. Expressing Y_ρ, Z_ρ as $Y_\rho = W_\rho + W_\rho^\dagger$, $Z_\rho = (W_\rho - W_\rho^\dagger)/i$, where W_ρ are complex matrices, and assuming that the Hamiltonian does not change under the above transformations, the condition is given as follows;

$$\{X, V\} + W_0^\dagger\Gamma_0 + \Gamma_0 W_0 = 0, \tag{122}$$
$$W_0^\dagger V + VW_0 = 0, \tag{123}$$
$$W_1^\dagger V + VW_1 + W_2\Gamma_0 + \Gamma_0 W_2^\dagger = 0, \tag{124}$$
$$W_2^\dagger V + VW_2 + W_1\Gamma_0 + \Gamma_0 W_1^\dagger = 0, \tag{125}$$
$$\{X, \Gamma_0\} + W_0 V + VW_0^\dagger = 0, \tag{126}$$
$$W_1 V + VW_1^\dagger = 0, \tag{127}$$
$$W_2 V + VW_2^\dagger = 0, \tag{128}$$
$$W_0^\dagger\Gamma_0 + \Gamma_0 W_0 = 0, \tag{129}$$
$$W_1^\dagger\Gamma_0 + \Gamma_0 W_1 = 0, \tag{130}$$
$$W_2^\dagger\Gamma_0 + \Gamma_0 W_2 = 0. \tag{131}$$

Here, supposing

$$X = \begin{pmatrix} 0 & -i & i \\ i & 0 & -i \\ -i & i & 0 \end{pmatrix}, \tag{132}$$

$$W_0 = \begin{pmatrix} 0 & -i & i \\ 0 & 0 & 0 \\ 0 & 0 & 0 \end{pmatrix},\ W_1 = \begin{pmatrix} 0 & 0 & 0 \\ i & 0 & -i \\ 0 & 0 & 0 \end{pmatrix},\ W_2 = \begin{pmatrix} 0 & 0 & 0 \\ 0 & 0 & 0 \\ -i & i & 0 \end{pmatrix}, \tag{133}$$

and substituting these X, W_ρ into the above conditions, it is shown that all conditions are satisfied.

References

[1] "Position space formulation for Dirac fermions on honeycomb lattice," Nucl. Phys. B Volume 885, August 2014, Pages 61-75, Masaki Hirotsu, Tetsuya Onogi, Eigo Shintani, http://www.sciencedirect.com/science/article/pii/S0550321314001564.

[2] K. S. Novoselov, A. K. Geim, S. V. Morozov, D. Jiang, Y. Zhang, S. V. Dubonos, I. V. Grigorieva, and A. A. Firsov, Science **306**, 666 (2004)

[3] K. S. Novoselov, D. Jiang, T. Booth, V.V. Khotkevich, S. M. Morozov, and A. K. Geim, Proc. Natl Acad. Sci. USA **102**, 10451 (2005), [cond-mat/0503533 [cond-mat.mtrl-sci]].

[4] K. S. Novoselov, A. K. Geim, S. V. Morozov, D. Jiang, M. I. Katsnelson, I. V. Grigorieva, S. V. Dubonos and A. A. Firsov, Nature **438**, 197 (2005), [cond-mat/0509330 [cond-mat.mes-hall]].

[5] Y. Zhang, Y. -W. Tan, H. L. Stormer and P. Kim, Nature **438**, 201 (2005).

[6] M. I. Katsnelson, K. S. Novoselov, and A. K. Geim, Nature Physics 2, 620 (2006), [cond-mat/0604323[cond-mat.mes-hall]]

[7] D. C. Elias, R. V. Gorbachev, A. S. Mayorov, S. V. Morozov, A. A. Zhukov, P. Blake, L. A. Ponomarenko, I. V. Grigorieva, K. S. Novoselov, F. Guinea and A. K. Geim, Nature Physics **8**, 172 (2012).

[8] A. K. Geim and K. S. Novoselov, Nature Materials **6**, 183 (2007)

[9] A. H. Castro Neto, F. Guinea, N. M. R. Peres, K. S. Novoselov and A. K. Geim, Rev. Mod. Phys. **81**, 109 (2009).

[10] V. N. Kotov, B. Uchoa, V. M. Pereira, A. H. C. Neto and F. Guinea, Rev. Mod. Phys. **84**, 1067 (2012) [arXiv:1012.3484 [cond-mat.str-el]].

[11] P. R. Wallace, Phys. Rev. **71**, 622 (1947).

[12] W. H. Lomer, Proc. Roy. Soc. (London) **330**, A227 (1955).

[13] J. C. Slonczewsky and P. R. Weiss, Phys. Rev. **109**, 272 (1958).

[14] J. W. McClure, Phys. Rev. **104**, 666 (1956).

[15] G. W. Semenoff, Phys. Rev. Lett. **53**, 2449 (1984).

[16] V. P. Gusynin, S. G. Sharapov and J. P. Carbotte, Int. J. Mod. Phys. B **21**, 4611 (2007) [arXiv:0706.3016 [cond-mat.mes-hall]].

[17] K. Asano and C. Hotta, Phys. Rev. B **83**, 245125 (2011).

[18] L. Susskind, Phys. Rev. D **16**, 3031 (1977).

[19] H. S. Sharatchandra, H. J. Thun and P. Weisz, Nucl. Phys. B **192**, 205 (1981).

[20] C. van den Doel and J. Smit, Nucl. Phys. B **228**, 122 (1983).

[21] M. F. L. Golterman and J. Smit, Nucl. Phys. B **245**, 61 (1984).

[22] H. Kluberg-Stern, A. Morel, O. Napoly and B. Petersson, Nucl. Phys. B **220**, 447 (1983).

[23] R. Brower, C. Rebbi and D. Schaich, PoS LATTICE **2011**, 056 (2011) [arXiv:1204.5424 [hep-lat]].

[24] P. V. Buividovich and M. I. Polikarpov, Phys. Rev. B **86**, 245117 (2012) [arXiv:1206.0619 [cond-mat.str-el]].

[25] J. E. Drut and T. A. Lähde, Phys. Rev. Lett. **102**, 026802 (2009); J. E. Drut and T. A. Lähde, Phys. Rev. B **79**, 165425 (2009).

[26] W. Armour, S. Hands, C. Strouthos, Phys. Rev. B **81**, 125105 (2010).

[27] P. V. Buividovich, E. V. Luschevskaya, O. V. Pavlovsky, M. I. Polikarpov and M. V. Ulybyshev, Phys. Rev. B **86**, 045107 (2012) [arXiv:1204.0921 [cond-mat.str-el]].

[28] E. Shintani and T. Onogi, arXiv:1203.1091 [hep-lat]; E. Shintani and T. Onogi, PoS LATTICE **2012**, 062 (2012) [arXiv:1211.6495 [hep-lat]].

[29] Y. Araki and T. Hatsuda, Phys. Rev. B **82**, 121403 (2010) [arXiv:1003.1769 [cond-mat.str-el]].

[30] M. Creutz, JHEP **0804**, 017 (2008) [arXiv:0712.1201 [hep-lat]].

[31] C. Herring, Phys. Rev. **52**, 365 (1937).

[32] S. Reich et al., Phys. Rev. B **66**, 035412 (2002)

[33] Tetsuya Onogi, Lattice 2014.

[34] Tsuneya Ando, and Mikito Koshino, J.Phys. Soc. Jpn. **78**104716(2009).

[35] Edward McCann, and Mikito Koshino, Rep. Prog. Phys. **76** 056503 (2013).